heritage

MDPI

Article

Silver-Doped TiO_2-PDMS Nanocomposite as a Possible Coating for the Preservation of Serena Stone: Searching for Optimal Application Conditions

Marwa Ben Chobba [1], Maduka L. Weththimuni [2,*], Mouna Messaoud [1], Jamel Bouaziz [1], Rached Salhi [1,3], Filomena De Leo [4], Clara Urzì [4] and Maurizio Licchelli [2]

1 Laboratory of Advanced Materials, National School of Engineering, University of Sfax, Box 1173, Sfax 3038, Tunisia
2 Department of Chemistry, University of Pavia, Via Taramelli 12, 27100 Pavia, Italy
3 Laboratory of Electrochemistry and Physicochemistry of Materials and Interfaces, University of Grenoble Alpes-Savoie Mont Blanc, Grenoble INP, 38000 Grenoble, France
4 Department of Chemical, Biological, Pharmaceutical and Environmental Sciences, Viale F. Stagno d'Alcontres, 31, 98166 Messina, Italy
* Correspondence: madukalankani.weththimuni@unipv.it

Abstract: The main objective of this research is to determine the optimal application conditions of a newly synthesized multifunctional coating containing Ag-doped TiO_2 nanoparticles when used as a possible protective agent for sandstone. Firstly, Ag-TiO_2 nanoparticles with anatase structure, spherical shape and controllable sizes were prepared using the sol–gel method and characterized. The biocidal activity of Ag-doped TiO_2 NPs was studied by comparing its performance to pure TiO_2 NPs against two representative Gram-positive and Gram-negative bacterial strains, under both visible irradiation and in the dark; then, the antimicrobial efficiency of two different concentrations of Ag-TiO_2 nanoparticles (0.1–1 mol%) was evaluated against two phototrophic strains commonly isolated from deteriorated surfaces. Results showed that the photoactivation and photokilling activity of TiO_2 were highly improved by doping with Ag. Next, prepared nanopowders were dispersed in a binder with different powder/PDMS ratios: (0.1, 0.2, 0.5 and 1% w/v TiO_2) and then applied in different amounts (2, 3 and 6 g/m^2) on Serena stone specimens. Results revealed that the application of 2 g/m^2 nanocomposite at powder/binder ratios equal to 1% w/v TiO_2 provided a fine hydrophobic character for the stone material with acceptable chromatic variations.

Keywords: Ag-doped TiO_2; nanoparticles; photocatalytic activity; antibacterial activity; Serena stone; stone conservation; heritage buildings

check for updates

Citation: Ben Chobba, M.; Weththimuni, M.L.; Messaoud, M.; Bouaziz, J.; Salhi, R.; De Leo, F.; Urzì, C.; Licchelli, M. Silver-Doped TiO_2-PDMS Nanocomposite as a Possible Coating for the Preservation of Serena Stone: Searching for Optimal Application Conditions. *Heritage* **2022**, *5*, 3411–3426. https://doi.org/10.3390/heritage5040175

Academic Editor: Chiara Soffritti

Received: 27 September 2022
Accepted: 4 November 2022
Published: 11 November 2022

Publisher's Note: MDPI stays neutral with regard to jurisdictional claims in published maps and institutional affiliations.

Copyright: © 2022 by the authors. Licensee MDPI, Basel, Switzerland. This article is an open access article distributed under the terms and conditions of the Creative Commons Attribution (CC BY) license (https://creativecommons.org/licenses/by/4.0/).

1. Introduction

Besides their historical relevance, heritage buildings have economic value due to their attractive architecture and important events that take place around the heritage sphere [1]. However, they are exposed to the degradation process and ageing. In particularly, microorganisms are usually related to the aggresive biodegradation of artistic materials [2,3]. Water is also an essential factor of deterioration, particularly in porous materials [4]. In addition to physical and chemical decay processes, water is essential for biodeteriogens whose growth contributes to stone artwork's decay. To protect heritage materials, several methods have been developed. Notably, the use of nanomaterials displaying self-cleaning features has been considered an interesting and cost-effective method for preserving valuable heritage surfaces [5]. In particular, TiO_2 nanoparticles (NPs) have been extensively regarded as one of the most interesting materials. Their self-cleaning properties are induced by a well-known photocatalytic mechanism. In general, the absorption of a photon with energy greater than the band gap energy results in the formation of a reactive oxygen

species (ROS) [6]. In particular, the hydroxyl radicals ($HO^{\bullet}$) revealed the highest oxidation potential (2.8 V), which makes them highly effective against the degradation of organic material and the inactivation of microorganisms [6]. Despite TiO_2 NPs efficiency, the rapid recombination of charge carriers and the requirement of the use of ultraviolet radiation as an excitation source prevent their widespread practical application [7]. Doping TiO_2 nanoparticles with noble metals is considered a good strategy for enhancing the performance of pure TiO_2 NPs. Schottky barriers, which are located at each Ag/TiO_2 contact region, are able to reduce the recombination of light-generated e^-/h^+ on the TiO_2's surface. Moreover, the Ag ions are recognized as being a powerful agent for inhibiting bacterial development [6]. In the field of the conservation of artwork materials, protective coatings with self-cleaning efficiencies have been developed to preserve precious stone-made historical materials [1,4–10]. However, few works have been written on the protection of heritage items constructed from Serena stone [11]. It is a sandstone with low porosity (5–10% open porosity), which is considered an important architectural and ornamental material in Italy. It is mainly composed of the elements Si (around 70% of the total weight) and O.

In this work, the efficiency of Ag-doped TiO_2 nanoparticles have been studied by evaluating as-prepared NP's performance in photodegrading pollutants under UV and visible light and inactivating bacteria under low-intensity artificial visible light, as well as in the dark. Methylene blue (MB) staining was used in this study to evaluate the photodegradation capacity of the obtained nanopowders. Antibacterial activity was evaluated against microbial strains *Stenotrophomonas maltophilia* (*S. maltophilia*), *Micrococcus luteus* (*M. luteus*) and *Chlorella* sp., and against a *Leptolynbya*-like filamentous cyanobacterium. The characteristics of as-synthesized NPs were evaluated by X-ray diffraction (XRD), Raman, transmission electron microscopy (TEM) and scanning electron microscopy (SEM) analyses. The following step of this research was based on studying the optimal conditions for applying a nanocomposite material as a protective coating on a Serena stone (SS) surface. As a preliminary study, the chromatic varitions, as well as hydrophobic properties of the newly synthesized material, were evaluated, because it was expected that the nanocomposite coating developed in this work would induce negligible colorimetric variations on the treated surface and exhibit good water-repellent features when applied to the stone surface. To accomplish this objective, NPs were dispersed in a binder (Polydimethylsiloxane, PDMS) with different powder/PDMS ratios (0.1, 0.2, 0.5 and 1% *w*/*v* TiO_2), and different amounts (2, 3 and 6 g/m^2) were applied to the Serena stone specimens. Chromatic variations before and after treatments, as well as hydrophobic features, were analyzed to determine the optimal conditions for nanocomposite application as a protective coating for Serena stone.

2. Material and Methods

2.1. NPs Preparation

The protocol of elaboration of bare and Ag-doped TiO_2 NPs is detailed in our prior research study [6]. The resulting nanopowders were post-heat treated with a heating rate of 5 °C/min until reaching 500 °C; then, NPs were maintained at that temperature for 2 h [12]. Post-heat treatment principally assists in eliminating leftover organic impurities, and increasing the crystallinity of the material, consequently enhancing the photoresponse activity of the obtained NPs [13].

2.2. Characterization of As-Prepared Nanoparticles

X-ray diffraction (XRD) was performed by a "BRUKER-AXS-D8-Advance" diffractometer instrument (Cu Kα radiation:λ = 1.5406 Å as ray source, 2θ range from 20° to 80°). Raman spectra were collected using a Horiba/Jobin Yvon Lab Ram spectrometer (laser excitation = 488 nm, exposure time = 2 s, resolution = 1 cm^{-1}:64 scans). SEM (backscattered electron, BSE mode) images were collected with a Tescan FE-SEM, MIRA XMU series (TESCAN, Brno, Czech Republic) equipped with a Schottky field emission source and located at the Arvedi Laboratory, CISRiC, University of Pavia, Pavia, Italy. Transmission

electron microscopy (TEM) and electron diffraction analyses were performed on an MET FEG JEOL 2010 microscope (operated at 200 kV with a 0.194 nm point-to-point resolution).

2.3. Photo-Degradation and Antimicrobial Tests

The self-cleaning efficiency of the obtained nanopowders was investigated by the degradation of methylene blue dye (MB, Dye content, ≥82%, Sigma Aldrich, Milan, Italy) under visible and UV irradiation by the presence of bare and doped NPs in methylene blue aqueous solution. The protocol of the self-cleaning test was already reported [14]. In this study, the apparent rate constant (K_{ap}) was calculated from the linear fitting of $\ln(C_0/C)$, presented in our previous work [6], versus th reaction time after 6 h.

The inactivation of two bacterial strains isolated from biodeteriorated surfaces, one Gram-negative (*Stenotrophomonas maltophilia* BC656) and the other Gram-positive (*Micrococcus luteus* BC657), was assessed at two contact times (12 and 24 h). In brief, each strain allowed to grow on a TSA medium for 24–48 h at 28 °C, and cells were harvested and suspended in distilled water to obtain an OD_{550} of 0.125, corresponding to a concentration of 1.5×10^8 cells/mL. Thirty µL of suspension was distributed into the wells of a test plate (24 wells, Orange Scientific), each containing 150 µL of TiO_2 or Ag-TiO_2 suspended in distilled water (2% *w*/*v*) and 120 µL of physiological solution (1.8% NaCl). The total amount in each well was 300 µL and the final bacterial concentration was 1.5×10^7 cell/mL, and the NPs-suspension concentration was equal to 1% *w*/*v*. Test plates were exposed in the presence of visible light and in parallel, a similar experiment was carried out in the dark. The test plates were kept, under continuous stirring, for 12 and 24 h. In order to evaluate the survival of cells, after each contact time, 1 mL of each suspension was diluted in decimal series and 10 µL of each bacterial suspension/dilution were inoculated in a suitable growth medium (TSA, Oxoid) and incubated at 28 °C for 48 h in order to evaluate the percentage of surviving cells compared to the controls (C_{SL}/C_D respectively bacterial suspension alone exposed under the visible lamp and in the dark).

The antimicrobial efficiency of 0.1–1% Ag-doped TiO_2 nanoparticles was also evaluated against a phototrophic mixture of eukaryotic alga *Chlorella* sp and a prokaryotic filamentous cyanobacterium *Leptolyngbya*-like strains, isolated from deteriorated stones, according to the following experimental conditions. Fresh cultures of each strain were obtained in BG11 liquid medium [15] after 15 days of incubation at room temperature of 26 °C and daylight under continuous rotation (50 rpm), after growth cell suspensions were centrifuged at 3500 rpm per 15 min, and then washed 3 times with PBS (Phosphate Buffer Saline). The pellet was resuspended in distilled water to obtain a final concentration of 1×10^5 cells/mL, which was determined by direct count under a microscope with a counting Burker chamber. The mixture was prepared by using an equal volume of each suspension. Paper discs (6 mm ∅) were imbibed with 100 µL of nanoparticles suspension (1 *w*/*v* % of colloidal suspension, composed of nanoparticles suspended in acetone) and allowed to dry.

The test was carried out by preparing tubes, each one containing 25 mL of melted agarized BG1 medium, kept at a temperature of 48 °C. Then, in each tube, 1 mL of as-prepared microbial suspension was added to the melted media. The mixture was vortexed gently and poured directly into the Petri dish. After the agarized medium was solidified, as-prepared discs soaked with colloidal suspension were placed on the surface of the solidified BG11 agar. As controls, discs were soaked with only distilled water 'H_2O' and only acetone 'Ac'. All experiments were carried out in duplicate. Petri dishes were exposed under a solar lamp (Radium Floradym Spot E27 R63). Inhibition areas were recorded after growth was visible around the controls.

2.4. Preparation and Application of Nanocomposite Protective Coatings on Stone Specimens

The application of newly synthesized coatings was performed on the standardized stone specimens (UNI 10 921 Protocol) [16]. For instance, Serena stone (SS) specimens (5 × 5 × 1 cm) were smoothed via the use of abrasive carbide paper (No: 180 mesh), washed with deionized water, dried in an oven at 60 °C, and stored in a desiccator [17,18].

Pure and doped TiO_2 NPs with different doping concentrations were mixed with polydimethylsiloxane (PDMS, HO[-Si(CH_3)$_2$O-]n H, M.W. 4200, Alfa Aesar, Kandel, Germany) in different powder/binder ratios (0.1, 0.2, 0.5 and 1% w/v). The homogenization of NPs in the binder matrix was performed usingan ultrasonic homogenizer (Bandelin SONOPULS HD 2070), as recommended in the literature [19,20]. Next, 1.5 g (±0.02) of each prepared formulation was applied to 25 cm^2 of SS specimens by the brushing method, as previously reported in our papers, and use in the real applications [6,20,21], which corresponds to an amount of nanoparticles equal to 6 g/m^2. Other series of samples were prepared by diluting PDMS with tert-butyl alcohol (TBA) at a dilution ratio equal to 1:10 (PDMS:TBA) and 0.5, 0.75 and 1.5 g of the resulting mixture was applied on 25 cm^2 SS surfaces which correspond to 2, 3 and 6 g/m^2. After applying different coatings, all SS specimens were kept to dry at room temperature (20 ± 2 °C) for at least 21 days.

Chromatic variations were measured by a Konica Minolta CM-2600D spectrophotometer, determining the L*, a*, and b* coordinates of the CIELAB space, and the global chromatic variations, expressed as ΔE* according to the UNI EN 15886 protocol [22]. The contact angle measurements were realized in order to determine the hydrophobic properties of the treated surfaces. The test was performed according to the Italian protocol UNI 11207:2007 [23] using a Lorentzen & Wettre instrument.

3. Results and Discussion

3.1. Characterization of As-Prepared NPs

In a previous work, the XRD patterns of pure and doped TiO_2 nanopowders showed that anatase phase with tetragonal geometry (JCPDS-782486) was obtained [6]. Based on the XRD data, the average crystallite, lattice parameters and lattice volume were estimated. The values related to all samples are illustrated in Table 1. After doping pure NPs with silver ions, a slight decrease in crystal size was observed; this fact demonstrates that silver ions slightly inhibit the crystal growth of pure TiO_2 NPs. The obtained results are in contrast with those reported by Pham and Lee [24] who stated that Ag^+ ions, when they are localized on the surface of TiO_2 NPs, are able to hinder the crystallization of the TiO_2 anatase phase. In our study, it can be revealed that doping TiO_2 by Ag ions slightly affects the lattice parameters and even the lattice volume of pure TiO_2 NPs. However, the detected reduction may be attributed to measurement and/or instrumental errors during the performance of the analysis. The negligible variation in lattice volumes after doping TiO_2 with silver ions suggests that Ag^+ is not inserted inside the TiO_2 lattice, as would be expected if the difference in ionic radius of Ti^{4+} (0.68 A°) and Ag^+ (1.26 A°) were to be considered [25]. Indeed, if this had happened, a volume inflation would have been noticed in Titanium dioxide lattice, which is not the case in this study. Although the replacement of Ti from its lattice by Ag requires an important amount of energy and is not easy because of the high ionic radius of silver ions (Ag^+) compared to Ti^{4+}, a small fraction of Ti^{4+} could be substituted by Ag^+, resulting in the formation of only small amounts of Ti^{3+} [24].

Additional data on the phase crystallinity of the obtained NPs is provided by Raman spectroscopy. Based on our previous work, the six Raman active modes (A1g + 2B1g + 3Eg) of TiO_2 anatase phase have been observed [6]. A shift in the signals, particularly in Eg mode, is observed as the Ag content increases in the samples. It appears that the Eg mode of TiO_2 was also observed to shift from 142.73 cm^{-1} to a higher wavenumber, and we expect that samples doped with 3 mol% Ag shift back to 142.9 cm^{-1} (Figure 1 and Table 2). It has been reported that the shift in the Raman peak might probably occur because of an alteration in the structure, the particle size and the nature of defects, etc. [26]. This alteration is due to the introduction of silver ions into TiO_2 network. Besides, a broadening

of the peaks, due to doping effect, can be observed in Figure 1a and was validated by the calculation of the full width at half maximum [FWHM] of the E_{1g} mode at 142 cm^{-1} (Table 2).

Table 1. Average crystallite sizes and lattice parameters of Ag-doped TiO_2 NPs.

Samples	D (nm)	a = b (Å)	C (Å)	c/a	V (Å^3)
Pure TiO_2	20 ± 2	3.793	9.518	2.509	136.93
0.1 mol% Ag-TiO_2	18 ± 1	3.790	9.509	2.508	136.58
1 mol% Ag-TiO_2	17 ± 1	3.781	9.486	2.508	136.61
3 mol% Ag-TiO_2	16 ± 2	3.786	9.484	2.505	135.94
5 mol% Ag-TiO_2	16 ± 1	3.784	9.483	2.506	135.67

D: the crystallite size; a, b and c: the parameters of the elementary cell of the quadratic system of anatase phase; V: the volume of the unit cell.

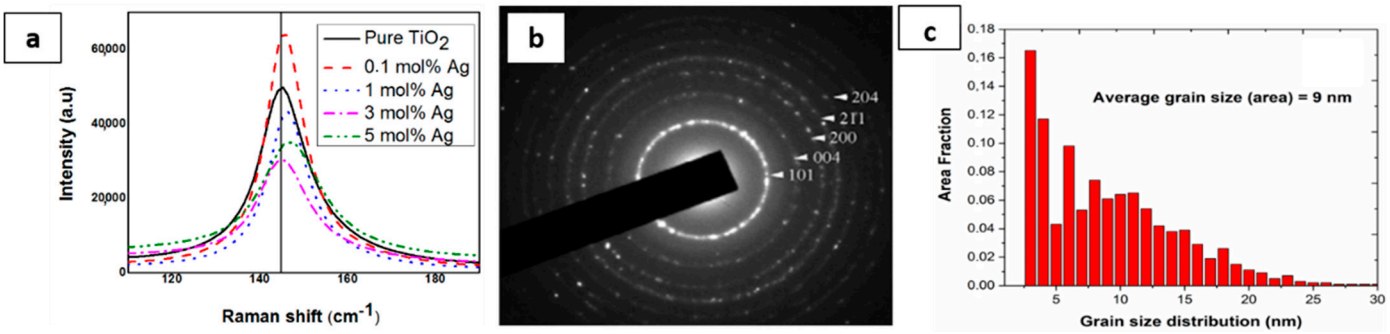

Figure 1. (**a**) The Raman-active mode of pure and doped TiO_2 at 142 cm^{-1}; (**b**) selected area electron diffraction pattens (SAED) where the diffraction planes correspond to the anatase structure of TiO_2 nanoparticles; and (**c**) grain size distribution.

Table 2. The position and FWHM of the E_{1g} mode for pure and Ag-doped TiO_2 nanoparticles.

Sample	Position of the E_{1g} Mode (cm^{-1})	FWHM (cm^{-1})
Pure TiO_2	142.73	10.66
0.1 mol% Ag-TiO_2	142.80	10.52
1 mol% Ag-TiO_2	143.87	11.20
3 mol% Ag-TiO_2	142.90	12.77
5 mol% Ag-TiO_2	144.28	15.40

E_{1g}: Raman active mode; FWHM: the full width at half maximum intensity.

The broadening of the Raman-active bands can be related to the concentration of oxygen vacancies on the photocatalysts [27]. In fact, the introduction of the dopant promotes the formation of oxygen vacancies on the oxide surface, raising system disorder. As previously mentioned, the substitution of Ti^{4+} by Ag^{+} on the surface of the photocatalyst would create oxygen vacancies. These oxygen vacancies are predicted to promote the separation of photo-generated charge carriers and consequently improve the photocatalytic activity. In fact, it was stated that oxygen vacancies and surface defects enhance electron-trapping and light-generated (e^{-}/h^{+}) separation processes [28]. The anatase crystal structure was validated by SAED technique; one SAED ring diffraction pattern with marked Miller indices of the anatase titanium dioxide nanoparticles (JCPDS Card No. 21-1272), as is shown in Figure 1b. The ring pattern proved that the resulting nanopowders are polycrystalline, while the grainy appearance of rings is related to the fact that the size of the constituent crystallites is in the range of 9 nm Figure 1c.

An SEM micrograph (Figure 2a) shows that pure TiO_2 nanopowders are constituted by agglomerated spheres with an approximate size of 500 µm. These spheres are formed from an enormous amount of small particles (10–20 nm), as can be revealed from Figure 2b.

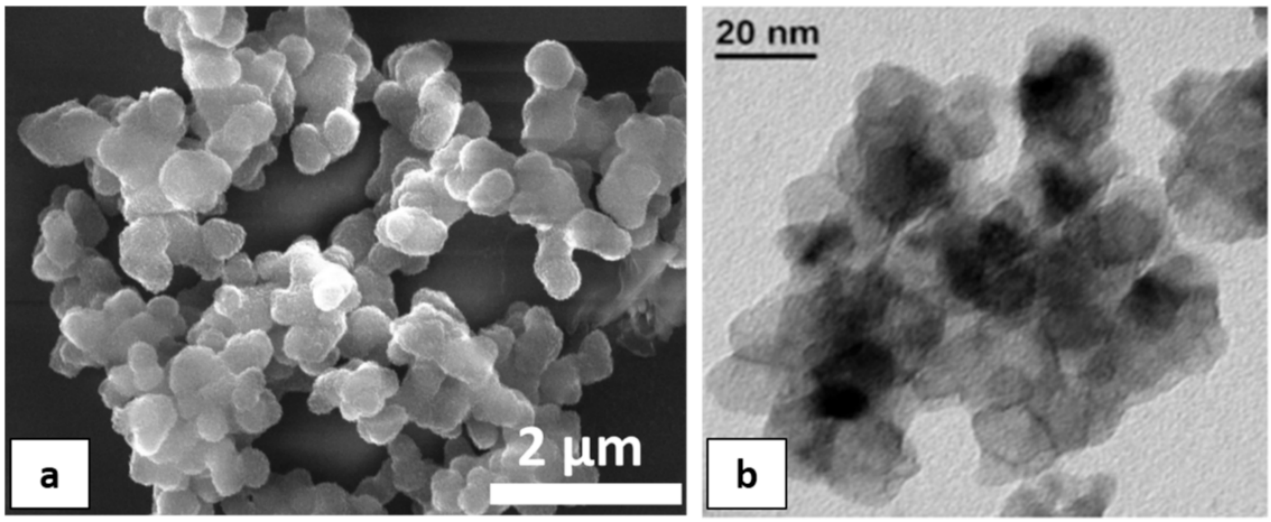

Figure 2. (**a**) SEM; and (**b**) TEM micrograph of pure TiO_2 nanoparticles.

3.2. Photocatalytic Degradation

The photo-degradation efficiency of pure/doped NPs with a different doping % of silver ions was evaluated through the photo-decomposition of the MB stain, under both UV and visible light irradiation. The K_{ap} values of the catalyst (Table 3) show that the decomposition of MB dye increases considerably with the incorporation of Ag ions. In fact, bare TiO_2 shows a very low decolorization rate, while the degradation rate constant (K_{ap}) for Ag-doped TiO_2 NPs is considerably increased. In particular, under UV irradiation, K_{ap} values are found to be increased by 2.6, 2.5, 2.3 and 2 times for samples doped with 0.1, 1, 3 and 5 Ag mol%, respectively, compared to pure TiO_2. Under the visible light, 0.1% doping induces the highest increase rate (by 4.4 times), while NPs doped with 1, 3 and 5 Ag mol% showed a comparable behavior with an average MB degradation rate constant 3.7 times larger than undoped TiO_2. Therefore, doping with the lowest Ag amount (0.1%) corresponds to the highest increase in the highest photo-degradation rate under visible and ultraviolet light illumination.

Table 3. Percentage degradation after exposure to UV and visible-light radiation and the apparent rate constant (K_{ap}).

Samples	K_{ap} [a] (h^{-1})		Band Gap Energy (e.v) [6]
	Under UV Light	Under Visible Light	
Pure TiO_2	0.102	0.044	3.25
0.1% Ag-TiO_2	0.265	0.185	2.71
1% Ag-TiO_2	0.246	0.161	2.65
3% Ag-TiO_2	0.232	0.162	2.59
5% Ag-TiO_2	0.201	0.167	2.57

[a] the apparent rate constant (K_{ap}) calculated from the linear fitting of $\ln(C_0/C)$ versus reaction time after 6 h.

In order to understand the photocatalytic process and the role of reactive species ($HO^{\bullet}$, h^{+}, $O_2^{\bullet}$) involved in the degradation of MB, Ali et al. [29] performed scavenger analysis. It is based on using scavengers, dissolved separately into the MB dye solution, to trap hydroxyl radicals ($HO^{\bullet}$), hole (h^{+}) and superoxide radicals ($O_2^{\bullet}$). Results showed that holes and superoxide radicals play little role in the degradation of MB dye, while hydroxyl radicals were the major active species. MB dye can be degraded by the photocatalysis process. When Ag-doped TiO_2 samples are exposed to visible illumination, an electron is transferred from the valance band (VB) of TiO_2 NPs to the localized states created by Ti^{3+}, and thereafter to the conduction band (CB) according to Equation (1), which might be transferred to the silver NPs deposited on the surface (Figure 3). The above processes would assure an effective separation of photogenerated positive and negative charge carriers.

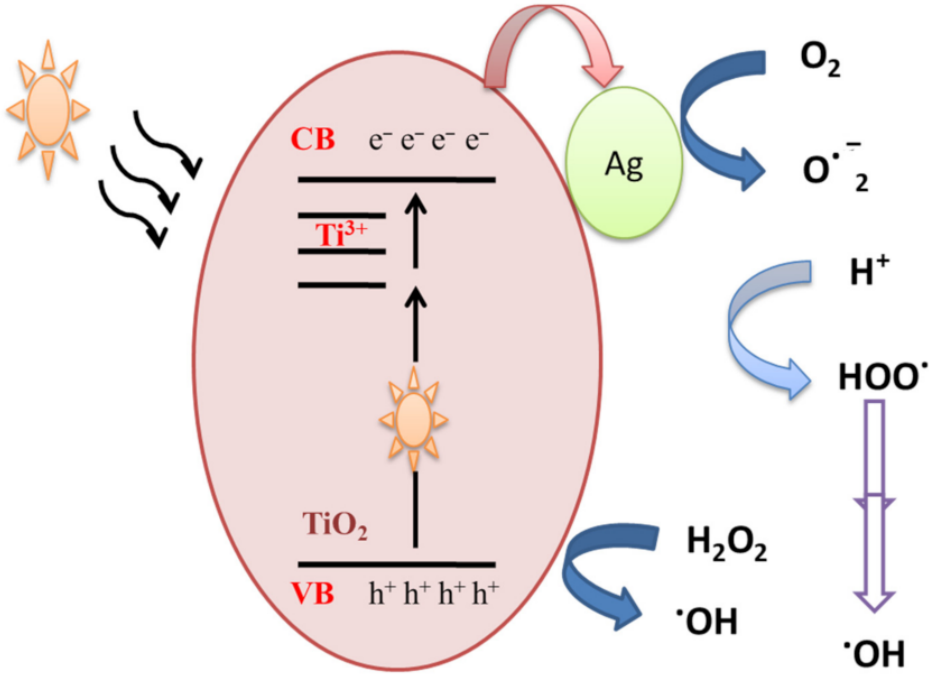

Figure 3. Mechanistic schematics of silver-doped TiO_2 NPs under visible illumination.

$$\text{Ag-TiO}_2 + h\nu \rightarrow \text{Ag-TiO}_2(\text{VB } h^{+}) + \text{Ag-TiO}_2(\text{CB } e^{-}) \quad (1)$$

The accumulated electrons in the TiO_2-Ag NPs react with adsorbed oxygen and produce ROS such superoxide anion $O_2^{-\bullet}$. On the other hand, hydroxyl radicals are produced due to a reaction between holes present in the valance band of TiO_2 and water molecules or the OH group. The generated hydroxyl radicals and separated charge carriers then contribute to the decomposition of organic pollutants.

3.3. Antibacterial Activity

The inactivation of Gram-negative and Gram-positive bacterial strains, after contact with pure and doped suspensions, was investigated under visible light and in the dark at two contact times (12 and 24 h). After each contact time, the bacteria was incubated at 28 °C during 48 h to determine the percentage of surviving cells. The results are illustrated in the histogram, as shown in Figure 4. Outcomes showed a significant difference in the antibacterial behavior of silver-doped TiO_2 NPs compared to pure NPs. In fact, a total inactivation of *S. maltophilia* was observed after being in contact with Ag-TiO_2 suspensions during 12 h under both visible irradiations and in the dark, regardless of the amount of silver ions, as can be shown in Figure 4a. After 12 h of contact, *M. luteus* inactivation was observed only after being in contact with both 3 and 5 mol% Ag-doped TiO_2 nanopowders in both working conditions (Figure 4b). The variation in the antibacterial ability with

Gram-positive strains has been exhibited by Ag-doped TiO_2 due to the varying amounts of Ag used for doping. The time required for the complete inactivation of *M. luteus* under solar light, after contact with 0.1–1 mol% Ag doped samples, was longer than the time required for *S. maltophilia* inactivation (24 h). Doping TiO_2 NPs with silver not only takes part in the improvement of the photo-response activity of nanoparticles, but also implemented their antibacterial performances. In fact, the inclusion of Ag ions added an extra antibacterial capability, in addition to those associated with TiO_2 photodegradation.

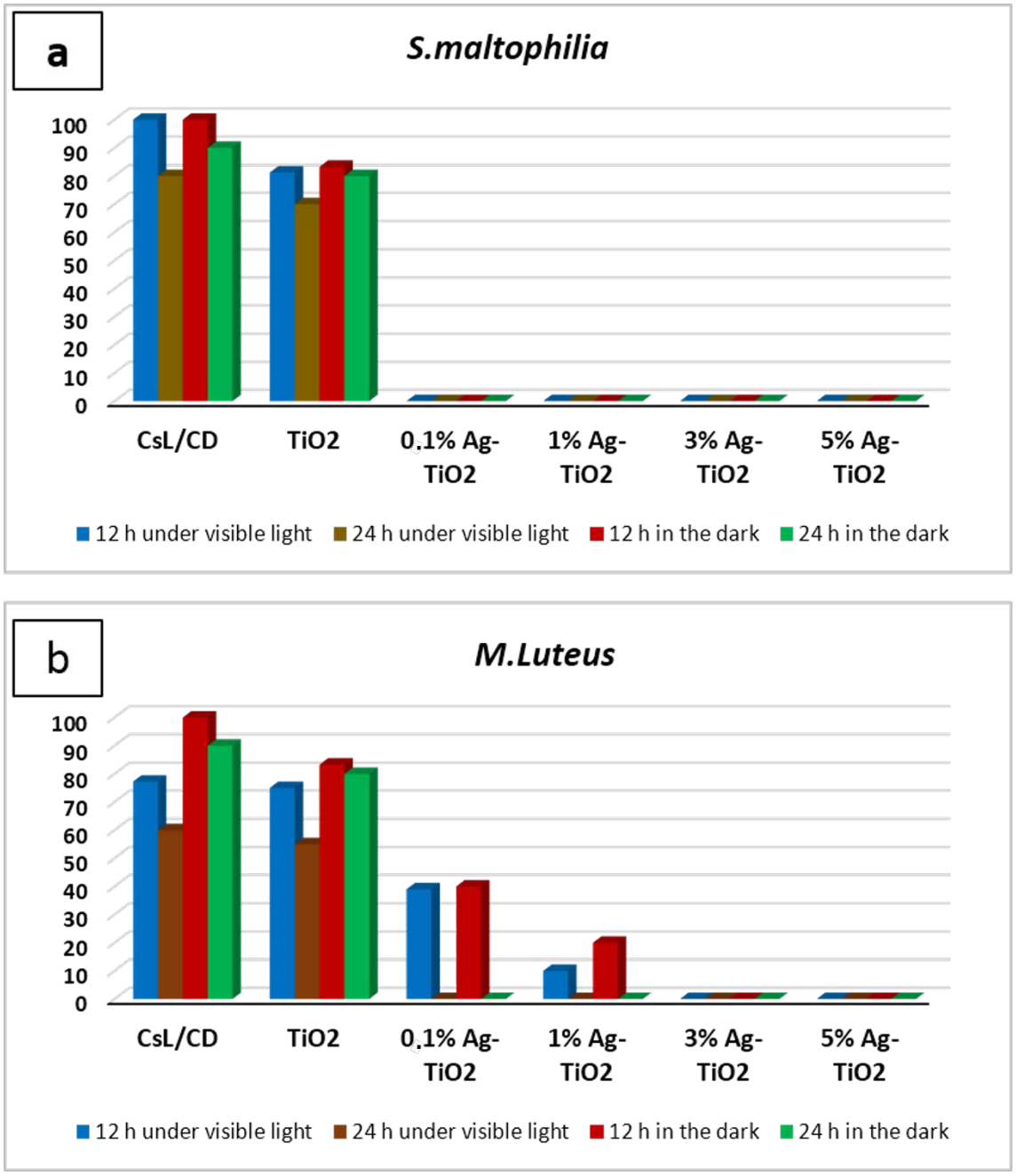

Figure 4. Antibacterial action tested with contact time technique against (**a**) *S. maltophilia*, (**b**) *M. Luteus* in different working conditions expressed as a percentage of surviving cells.

After 15 days, some colonies started to grow near the controls and 0.1% Ag-TiO_2 nanoparticles (Figure 5), whereas no growth was observed near 1%Ag-TiO_2 NPs. These findings reveal the efficiency of 1 mol% Ag-TiO_2 NPs in inhibiting microbial growth.

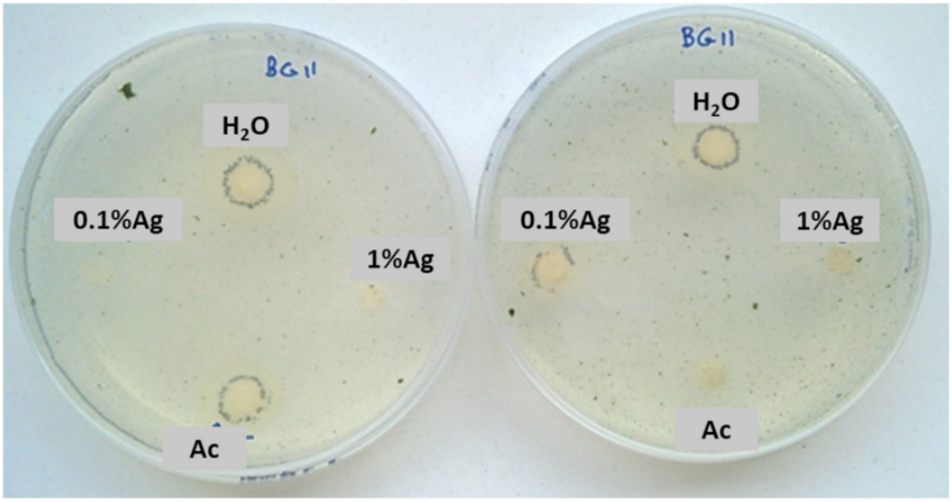

Figure 5. Sensitivity test carried out with a mixture of two phototrophic microorganisms exposed to solar lamp—*Chlorella* sp. and *Leptolyngbya*-like strains.

The antibacterial activity of silver ions has been studied for a long time in detail [30,31]. It was reported that silver ions are known to induce denaturation of proteins present in bacterial cell walls and inhibit bacterial growth [32]. Denaturation of proteins is a process in which proteins lose their native state due to some external stress, such as radiation, heat or notable compound, resulting in the disruption of cell activity and possibly cell death. Lehninger et al. [33] reported that silver ions interact with proteins by reacting with the sulfhydryl (SH) groups present in bacteria, inducing the inactivation of the proteins. Indeed, the primary molecular target for silver ions resides in cellular -SH groups, which are of ultimate importance for the activity of many enzymes and protein structures [34]. A further study performed by Liau et al. [35] stated that the interaction of Ag^+ with thiol groups played an essential role in bacterial inactivation. In fact, Ag ions may participate in photocatalytic oxidation reactions between oxygen molecules in the cell and thiol groups, promoting the formation of disulfide bonds (R-S-S-R) [29], and consequently causing the blocking of respiration and the cell death of the bacteria [36]. More recently, Feng et al. [37] studied the antibacterial activity of Ag^+ ions against a Gram-negative (*E. coli*) and Gram-positive (*S. aureus*) bacteria. Results revealed the existence of silver and sulfur elements in the cytoplasm. Moreover, a high amount of phosphorus, the primary component of DNA molecules, was detected in the middle of the cells. Therefore, it was believed that DNA loses its replication ability and cellular proteins become inactivated due to Ag^+ treatment. Another report announced that, in addition to the fact that silver ions inhibit several functions in the cell and consequently induce their damage, the generation of reactive oxygen species, possibly produced as a result of the respiratory inhibition of the enzyme(s) by silver ions, contributes to the attack of the cell itself [38].

3.4. Application of Protective Coatings on Serena Stone Specimens

As a first step, nanoparticles were mixed with PDMS at different powder/PDMS ratios (0.1, 0.2, 0.5 and 1% *w*/*v* TiO_2) to investigate the effect of nanopowder concentrations on the chromatic and hydrophobic features of tested stones. The different formulations were applied to the SS specimens (1.5 g of each formulation corresponds to 6 g/m^2), and results showed that all coatings displayed water-repellent features ($\alpha > 90°$) but unacceptable chromatic variations, since ΔE^* was above the recommended standard value ($\Delta E^* < 5$), as shown in Table 4 [17].

Table 4. Overall chromatic (ΔE*) and contact angle variations (α) of different samples.

Samples	ΔE*	α (°)
P	12.13 ± 0.6	111 ± 5
P + 0.1 Ti	13.03 ± 0.3	111 ± 4
P + 0.2 Ti	13.51 ± 0.5	100 ± 6
P + 0.5 Ti	12.25 ± 0.3	100 ± 2
P + 1 Ti	9.52 ± 1.5	114 ± 10

In order to deeply understand the influence of nanocomposite thin films on each chromatic coordinate (L*, a*, b*) of SS, results are graphically presented in Figure 6. The ΔL*, Δa* and Δb* values correspond to the difference between the value of each chromatic coordinate of the stone specimen before and after treatment. Results showed that L* is the most affected chromatic coordinate by all the applications of PDMS while b* and a* underwent less significant variations. Outcomes also indicate that ΔL* assumes negative values, which means that the applied coating caused a darkening of the SS surface. After introducing TiO_2 NPs into the binder, ΔL* showed only a slight variation compared to the plain binder, suggesting that PDMS is mainly responsible for the SS chromatic coordinate alterations. Particularly, samples treated with the highest NPs concentration showed the lowest ΔL* alteration. Considering these outcomes, we decided to perform additional experiments with a nanocomposite containing 1% w/v NPs, and to dilute it before application with an appropriate solvent in order to moderate the darkness induced by the polymer on the stone surface. Moreover, concerning the doped material, we focused on the material containing 1 mol% Ag-TiO_2 NPs, since they showed optimal performances in terms of (i) microbial inhibitor behavior (see Figure 4) and (ii) photocatalytic effect under both UV and visible light irradiation (see Table 3). In addition, the corresponding nanocomposite provided less drastical chromatic variation in the substrate, compared to the other tested materials containing doped NPs with different Ag contents.

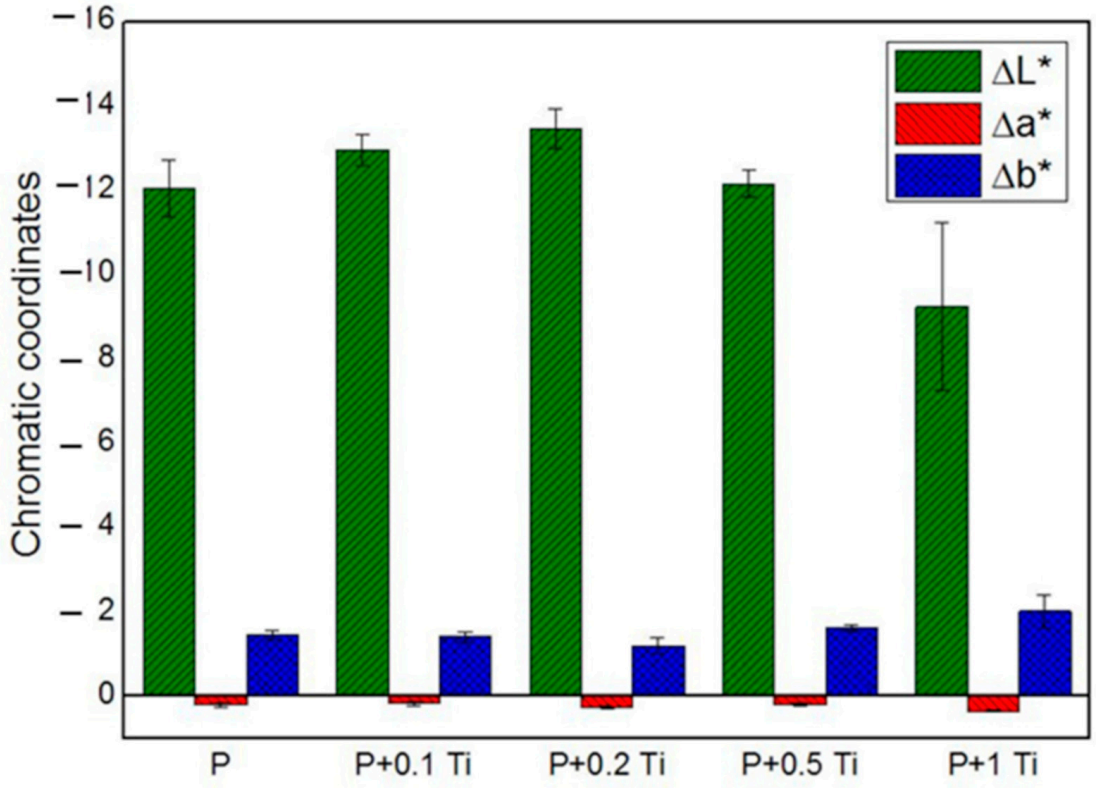

Figure 6. Chromatic coordinates of treated SS stones.

As a second step, PDMS was mixed with *t*-butanol at 1:10 ratio, and 1.5 g of the resulting product (corresponding to 6 g/m^2) was applied to SS specimens. The same dilution was performed even for all corresponding nanocomposites. The obtained findings of the contact angle and chromatic changes measurements are resumed in Table 5. All treatments, even with diluted PDMS, provided a contact angle higher than 90°, which reflects the hydrophobic character of the resulting coatings. It is worth noting that PDMS coatings are hydrophobic, and based on the obtained results, the addition of nanoparticles does not exhibit a significant variation in the hydrophobic character of coatings. However, it can be also deduced that dilution of PDMS was not sufficient to obtain acceptable chromatic variation, as suggested by ΔE* values (ΔE* = 6–11). Here also, it can be mentioned that the L* is the most affected chromatic coordinate, and it shifted to having positive values (i.e., lightness) when samples were treated with PDMS/TBA + 1 mol% Ag-TiO_2 NPs. The variation in b* is more relevant in this case as it moved from the blue to yellow color, since only negative Δb* values were obtained, particularly in the presence of NPs.

Table 5. The variation in color coordinates (ΔL*, Δa*and Δb*), overall chromatic and contact angle variations of treated SS specimens after dilution with *t*-Butyl alcohol.

Samples	ΔL*	Δa*	Δb*	ΔE*	α (°)
P	−10.7 ± 0.47	0.064 ± 0.029	−1.64 ± 0.15	10.83 ± 0.45	94 ± 6
P + 1% Ti	−6.93 ± 0.83	−0.026 ± 0.056	−3.63 ± 0.23	7.84 ± 0.61	100 ± 6
P + 1%Ti (1%Ag)	5.19 ± 0.76	−0.16 ± 0.0.03	−4.13 ± 0.23	6.64 ± 0.61	102 ± 1

In order to verify if lower amount can reduce the ΔL* induced by PDMS, we decided to test lower amounts of applied product; thus, the protective coating (PDMS: *t*-butanol 1:10) was applied according to 2 and 3 g/m^2, in addition to the amount already considered (6 g/m^2). Interestingly, samples treated with the lowest amount caused acceptable color modification, as can be proved by ΔE* values that are lower than or equal to 3 (Table 6). Decreasing the polymer amount applied did not significantly affect the water-repellent features of the coatings that showed contact angle values greater than 90° as can be revealed from Table 6, approving the hydrophobic behavior of the treated stone surface.

Table 6. The variation in color coordinates (ΔL*, Δa*and Δb*), overall chromatic and contact angle variation in treated SS specimens, after applying different amounts of PDMS: TBA (1:10.)

Applied Amount (g/m^2)	ΔL*	Δa*	Δb*	ΔE*	α (°)
6	−10.7 ± 0.47	0.064 ± 0.029	−1.64 ± 0.15	10.83 ± 0.45	94 ± 6
3	−8.28 ± 0.45	−0.086 ± 0.052	−1.86 ± 0.33	8.51 ± 0.47	102 ± 4
2	−2.16 ± 0.68	0.22 ± 0.072	−1.47 ± 0.1	3.02 ± 0.5	100 ± 1

Based on the obtained findings, we decided to set the applied amount at 2 g/m^2 and the powder/binder ratio at 1% *w*/*v* and then investigate the suitability of PDMS, mixed with neat and 1 mol% Ag-TiO_2 NPs at these conditions. Results showed that all treated samples exhibited water-repellent characteristics (i.e., α above 90°) and color alteration lower than 5 (Figure 7), which is considered to be lower than the limit for human eye perception [17].

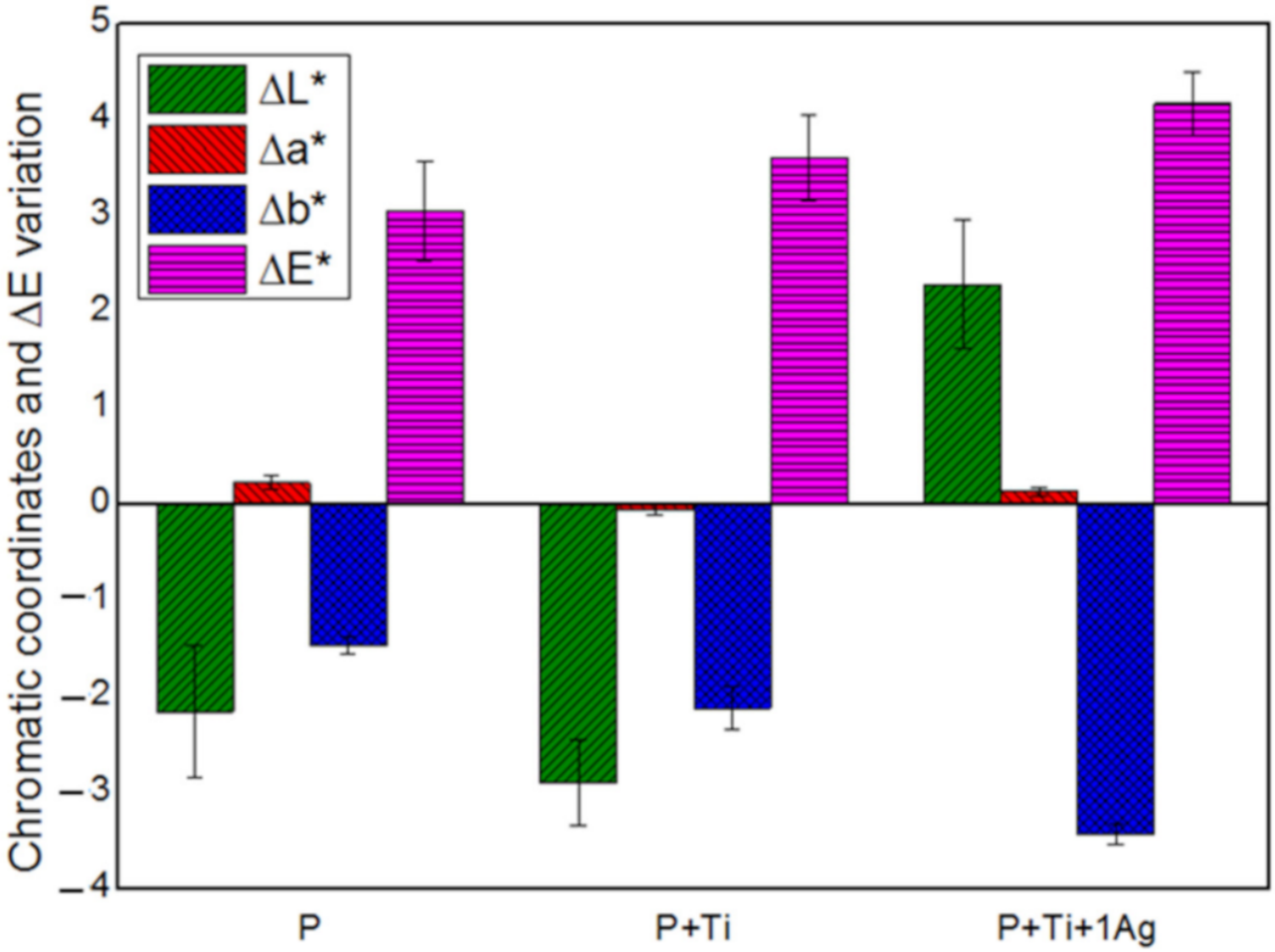

Figure 7. Chromatic coordinates and the overall chromatic variation in treated SS stones.

From these results, we can conclude that working with diluted PDMS (with TBA), applying only 2 g/m^2 of product and fixing NPs/binder ratios at 1% w/v are the optimal conditions to obtain an appropriate nanocomposite coating for the preservation of Serena stone-made historical materials.

In order to investigate the distribution of the nanoparticles (doped NPs with the binder) on the Serena stone surface, SEM analysis was performed, and the obtained results were reported in the Figure 8. For instance, it clearly showed the changes that appeared on the stone surface after the application of the protective coating (Figure 8c,d). As mentioned in the introduction, Serena stone is a sandstone which has low porosity (5–10%), and its natural morphology can be easily observed in Figure 8a,b. Moreover, a higher magnification image clearly showed the grains in the Serena matrix to be made of silicates and/or Quartz (with the chemical formula SiO_2). On the contrary, the doped NPs-PDMS treatment homogeneously dispersed on the stone surface by covering those silicate grains as well as the other compounds present on the stone surface, which provided good protective coating to the Serena stone. In addition, the higher magnification image shows how doped NPs englobed inside the polymer matrix by conjugating each other, which provided the good coating layer to the stone surface as reported in our previous papers (Figure 8d) [1,6].

All the results obtained from the preliminary analyses enabled us to understand the acceptable proportions and the suitable amount of nanocomposite material when it is applied as a protective coating to the Serena stone surface. As reported in our previous papers [1,6,7], further analyses should be performed to confirm the protecting effectiveness of this coating on this type of stone. Further experimental work on this is in progress in the laboratory.

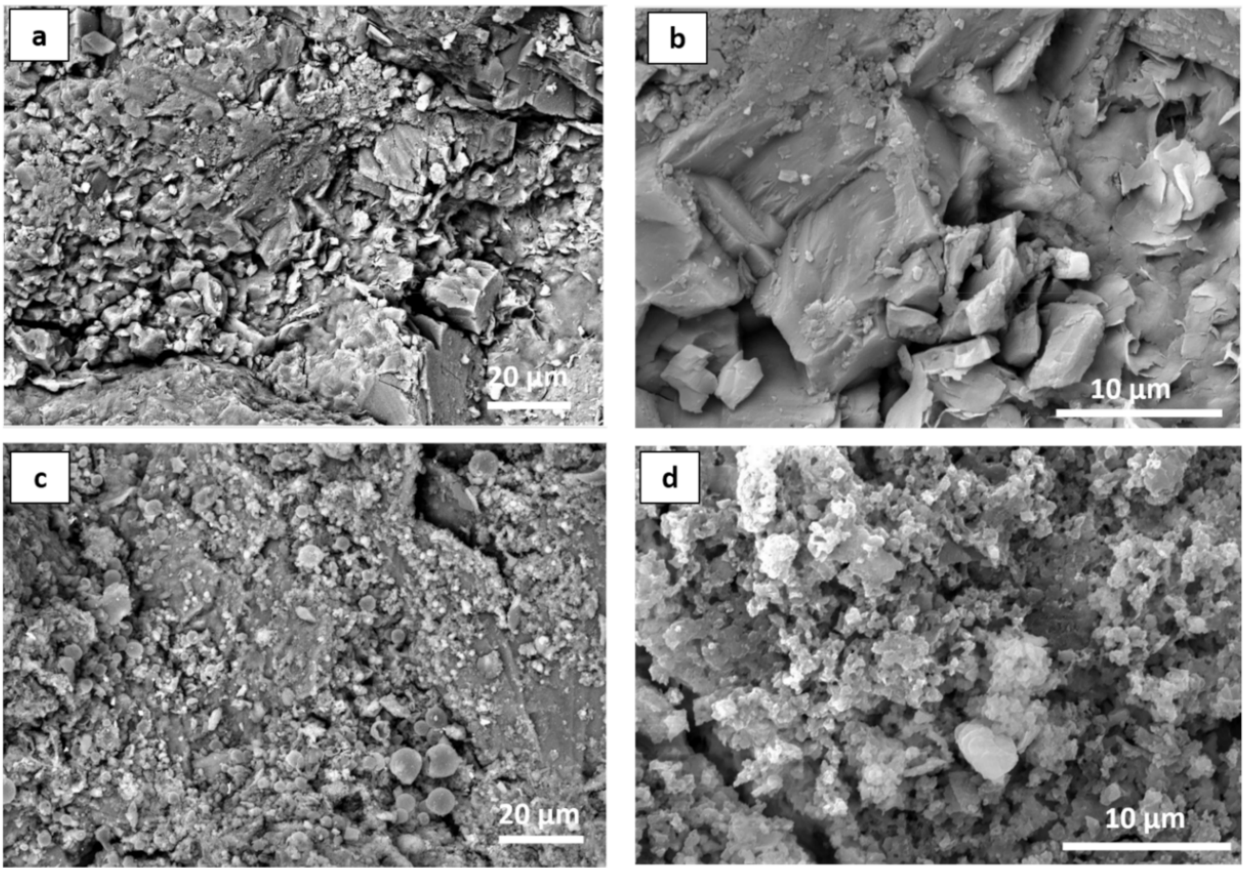

Figure 8. SEM micrographs of Serena stone (**a**,**b**) before treatment, and (**c**,**d**) after the application of 1 mol% Ag-TiO_2 NPs PDMS binder at the optimum conditions, at different magnifications.

The performance of the self-cleaning effect and anti-microbial effect is expected to be the same, since the PDMS binder did not affect the photocatalytic and the photo-killing performances of 1 mol% Ag-TiO_2 NPs, as reported in our previous work [6]. Results showed that the hydrophobic character of PDMS makes the microbial suspensions form a droplet shape on the stone surface, and prevent them from spreading overall across the stone surface; therefore, biofilm was formed only where the drops were present. On the other hand, PDMS, due to its water-repellent performance, prevents MB dye from penetrating inside the pores, and a stain remained on the surface making degradation more feasible. The outcomes showed clearly that the properties given by the NPs were not affected by the stone substrates. Nevertheless, the self-cleaning performances of nanocomposite-coated Serena stone are under investigation.

On the other hand, all our previous studies [1,6,7] suggested that doped NPs with PDMS (ZrO_2-ZnO-PDMS, Ag-TiO_2-PDMS, and Gd-TiO_2-PDMS) coating provided good protective properties to the considered stone substrates (Lecce stone, Marble, Bricks) for a long time without changing self-cleaning properties (the photo-protection and anti-microbial properties). It means that, when NPs ARW englobed in the polymer matrix, they create bonds with PDMS due to the presence of hydroxyl groups. So, they have no ability to easily move, and they stay with a binder material (PDMS). PDMS binds with stone matrix as a coating, together with NPs. In fact, until the coating decays, the NPs stay with PDMS, and they are neither able to go inside the stone matrix nor to the environment alone. As another old polymer coating (acrylic polymer: Paraloid B-72), it can probably be removed using emulsion, in the cleaning process which is commonly performed before restoration of the artefacts. However, the long-time investigation needs to confirm this process, and we are progressing our analysis on these points.

4. Conclusions

Neat and silver-doped TiO_2 nanopowders have been successfully prepared by one-step sol–gel process. Nanoparticles with anatase structure, spherical morphology and a size of about 20 nm were obtained. Outcomes revealed that introducing Ag ions into the structure of TiO_2 NPs would significantly improve the self-cleaning activity of nanopowders under visible and dark conditions. Doped NPs exhibited strong photo-killing activities under both visible conditions and in the dark by inactivating tested strains after 24 h of contact, regardless of the doping amount. Moreover, 1 mol% Ag-TiO_2 NPs exhibited efficient antimicrobial performances. As a next step, preliminary experimental analysis was performed on Serena stone specimens in order to evaluate the optimal application conditions of synthesized NPs dispersed in the PDMS binder as a protective coating on the sandstone materials. For this purpose, pure TiO_2 NPs were mixed with PDMS and the obtained nanocomposite was applied to the Serena stone surfaces at different NPs/PDMS ratios (0, 0.1, 0.2, 0.5 and 1% w/v). All coatings revealed ΔE^* higher than 5, which corresponds to color changes that can be detected by the naked eye. In particular, samples treated with a concentration of NPs equal to 1% (w/v) showed the lowest chromatic alteration. Thus, this ratio was used for the following work. In order to reduce the darkness induced by the polymer, PDMS was diluted with TBA at a dilution ratio equal to 1:10 (PDMS:TBA). Different quantities (i.e., 2, 3 and 6 g/m^2) of the prepared mixture were applied to the SS specimens. All coatings developed in this work showed water-repellent character, although only samples treated with the lowest quantity exhibited acceptable chromatic variation. Hence, this study indicated the optimal conditions to be used for the application of nanocomposite materials based on PDMS and pure and doped NPs (0.1–1 mol% Ag) as a promising protective coating for heritage Serena stone buildings. Further studies must be performed to confirm that the same performances are obtained from the nanocomposite coating on the treated Serena stone.

Author Contributions: Conceptualization, M.B.C., M.L.W. and M.L.; methodology, M.B.C., M.L.W., R.S., F.D.L. and C.U.; validation, M.L.W., C.U., J.B. and M.M.; formal analysis, R.S., C.U. and F.D.L.; investigation, M.B.C. and F.D.L.; resources, M.L., C.U., J.B. and M.M.; data curation, M.L.W.; supervision, M.M., M.L., M.L.W. and C.U.; writing—original draft preparation, M.B.C.; writing—review and editing, M.L.W., M.L. and C.U. All authors have read and agreed to the published version of the manuscript.

Funding: This research received no external funding.

Institutional Review Board Statement: Not applicable.

Data Availability Statement: Not applicable.

Acknowledgments: The authors gratefully acknowledge Ilenia Tredici, CISRiC, the University of Pavia, for handling the SEM–EDS analysis.

Conflicts of Interest: The authors declare no conflict of interest.

References

1. Weththimuni, M.L.; Ben Chobba, M.; Sacchi, D.; Messaoud, M.; Licchelli, M. Durable Polymer Coatings: A Comparative Study of PDMS-Based Nanocomposites as Protective Coatings for Stone Materials. *Chemistry* **2022**, *4*, 60–76. [CrossRef]
2. Russa, M.F.L.; Macchia, A.; Ruffolo, S.A.; Leo, F.D.; Barberio, M.; Barone, P.; Crisci, G.M.; Urzì, C. Testing the Antibacterial Activity of Doped TiO_2 for Preventing Biodeterioration of Cultural Heritage Building Materials. *Int. Biodeterior. Biodegrad.* **2014**, *96*, 87–96. [CrossRef]
3. Weththimuni, M.L.; Canevari, C.; Legnani, A.; Licchelli, M.; Malagodi, M.; Ricca, M.; Zeffiro, A. Experimental Characterization of Oil-Colophony Varnishes: A Preliminary Study. *Int. J. Conserv. Sci.* **2016**, *7*, 813–826.
4. Russa, M.F.L.; Rovella, N.; de Buergo, M.A.; Belfiore, C.M.; Pezzino, A.; Crisci, G.M.; Ruffolo, S.A. Nano-TiO_2 Coatings for Cultural Heritage Protection: The Role of the Binder on Hydrophobic and Self-Cleaning Efficacy. *Prog. Org. Coat.* **2016**, *91*, 1–8. [CrossRef]
5. Weththimuni, M.; Ben Chobba, M.; Tredici, I.; Licchelli, M. Polydimethylsiloxane (PDMS)/ZrO_2-Doped ZnO Nanocomposites as Protective Coatings for Stone Materials. In Proceedings of the 2020 IMEKO TC-4 International Conference on Metrology for Archaeology and Cultural Heritage, Tento, Italy, 16 October 2020.

6. Chobba, M.B.; Weththimuni, M.L.; Messaoud, M.; Urzi, C.; Bouaziz, J.; Leo, F.D.; Licchelli, M. Ag-TiO_2/PDMS Nanocomposite Protective Coatings: Synthesis, Characterization, and Use as a Self-Cleaning and Antimicrobial Agent. *Prog. Org. Coat.* **2021**, *158*, 106342. [CrossRef]
7. Ben Chobba, M.; Weththimuni, M.L.; Messaoud, M.; Sacchi, D.; Bouaziz, J.; De Leo, F.; Urzi, C.; Licchelli, M. Multifunctional and Durable Coatings for Stone Protection Based on Gd-Doped Nanocomposites. *Sustainability* **2021**, *13*, 11033. [CrossRef]
8. Domínguez, M.; Zarzuela, R.; Moreno-Garrido, I.; Carbú, M.; Cantoral, J.M.; Mosquera, M.J.; Gil, M.L.A. Anti-Fouling Nano-Ag/SiO_2 Ormosil Treatments for Building Materials: The Role of Cell-Surface Interactions on Toxicity and Bioreceptivity. *Prog. Org. Coat.* **2021**, *153*, 106120. [CrossRef]
9. Zarzuela, R.; Moreno-Garrido, I.; Gil, M.L.A.; Mosquera, M.J. Effects of Surface Functionalization with Alkylalkoxysilanes on the Structure, Visible Light Photoactivity and Biocidal Performance of Ag-TiO_2 Nanoparticles. *Powder Technol.* **2021**, *383*, 381–395. [CrossRef]
10. Weththimuni, M.; Ben Chobba, M.; Tredici, I.; Licchelli, M. ZrO2-Doped ZnO-PDMS Nanocomposites as Protective Coatings for the Stone Materials. *ACTA IMEKO* **2022**, *11*, 5. [CrossRef]
11. Bellissima, F.; Bonini, M.; Giorgi, R.; Baglioni, P.; Barresi, G.; Mastromei, G.; Perito, B. Antibacterial Activity of Silver Nanoparticles Grafted on Stone Surface. *Environ. Sci. Pollut. Res.* **2014**, *21*, 13278–13286. [CrossRef]
12. Ben Chobba, M.; Messaoud, M.; Bouaziz, J.; De Leo, F.; Urzì, C. The Effect of Heat Treatment on Photocatalytic Performance and Antibacterial Activity of TiO_2 Nanoparticles Prepared by Sol-Gel Method. In *Advances in Materials, Mechanics and Manufacturing*; Chaari, F., Barkallah, M., Bouguecha, A., Zouari, B., Khabou, M.T., Kchaou, M., Haddar, M., Eds.; Springer International Publishing: Cham, Switzerland, 2020; pp. 71–79. [CrossRef]
13. Ben Chobba, M.; Weththimuni, M.L.; Messaoud, M.; Bouaziz, J.; Licchelli, M. Enhanced Gd Doped TiO_2 NPs-PDMS Nanocomposites as Protective Coatings for Bio-Calcarenite Stone: Preliminarily Analysis. In *Design and Modeling of Mechanical Systems—V*; Walha, L., Jarraya, A., Djemal, F., Chouchane, M., Aifaoui, N., Chaari, F., Abdennadher, M., Benamara, A., Haddar, M., Eds.; Springer International Publishing: Cham, Switzerland, 2022; pp. 885–893. [CrossRef]
14. Ben Chobba, M.; Messaoud, M.; Weththimuni, M.L.; Bouaziz, J.; Licchelli, M.; De Leo, F.; Urzì, C. Preparation and Characterization of Photocatalytic Gd-Doped TiO_2 Nanoparticles for Water Treatment. *Environ. Sci. Pollut. Res.* **2019**, *26*, 32734–32745. [CrossRef]
15. Rippka, R.; Deruelles, J.J.B.W.; Waterbury, J.; Herdman, M.; Stanier, R. Generic Assignments, Strain Histories and Properties of Pure Cultures of Cyanobacteria. *Microbiol.-Sgm* **1979**, *111*, 1–61. [CrossRef]
16. *UNI 10921:2001*; Beni Culturali—Materiali Lapidei Naturali Ed Artificiali—Prodotti Idrorepellenti—Applicazione Su Provini e Determinazione in Laboratorio Delle Loro Caratteristiche. UNI: Milan, Italy, 2001. Available online: https://www.Biblio.Units.It/SebinaOpac/Resource/Beni-Culturali-Materiali-Lapidei-Naturali-Ed-Artificiali-Prodotti-Idrorepellenti-Applicazione-Su-pro/TSA1388731 (accessed on 30 September 2021).
17. Weththimuni, M.L.; Crivelli, F.; Galimberti, C.; Malagodi, M.; Licchelli, M. Evaluation of Commercial Consolidating Agents ON very Porous Biocalcarenite. *Int. J. Conserv. Sci.* **2020**, *11*, 251–260.
18. Weththimuni, M.L.; Licchelli, M.; Malagodi, M.; Rovella, N.; Russa, M.L. Consolidation of Bio-Calcarenite Stone by Treatment Based on Diammonium Hydrogenphosphate and Calcium Hydroxide Nanoparticles. *Measurement* **2018**, *127*, 396–405. [CrossRef]
19. Weththimuni, M.L.; Capsoni, D.; Malagodi, M.; Milanese, C.; Licchelli, M. Shellac/Nanoparticles Dispersions as Protective Materials for Wood. *Appl. Phys. A* **2016**, *122*, 1058. [CrossRef]
20. Weththimuni, M.L.; Milanese, C.; Licchelli, M.; Malagodi, M. Improving the Protective Properties of Shellac-Based Varnishes by Functionalized Nanoparticles. *Coatings* **2021**, *11*, 419. [CrossRef]
21. Ricca, M.; Le Pera, E.; Licchelli, M.; Macchia, A.; Malagodi, M.; Randazzo, L.; Rovella, N.; Ruffolo, S.A.; Weththimuni, M.L.; La Russa, M.F. The CRATI Project: New Insights on the Consolidation of Salt Weathered Stone and the Case Study of San Domenico Church in Cosenza (South Calabria, Italy). *Coatings* **2019**, *9*, 330. [CrossRef]
22. *UNI EN 15886:2010*; Conservazione DEI Beni Culturali, Metodi Di Prova, Misura Del Colore Delle Superfici. UNI Ente Italiano Di Normazione: Milan, Italy, 2010. (In Italian)
23. *UNI 11207:2007*; Beni Culturali—Materiali Lapidei Naturali Ed Artificiali—Determinazione Dell'angolo Di Contatto Statico Su Provini Di Laboratorio. UNI: Milan, Italy, 2007. (In Italian)
24. Pham, T.-D.; Lee, B.-K. Effects of Ag Doping on the Photocatalytic Disinfection of E. Coli in Bioaerosol by Ag–TiO_2/GF under Visible Light. *J. Colloid Interface Sci.* **2014**, *428*, 24–31. [CrossRef]
25. Kumaresan, L.; Palanisamy, B.; Palanichamy, M.; Murugesan, V. The Syntheses, Characterizations, and Photocatalytic Activities of Silver, Platinum, and Gold Doped TiO_2 Nanoparticles. *Environ. Eng. Res.* **2011**, *16*, 81–90. [CrossRef]
26. Xu, C.; Zhang, P.; Yan, L. Blue Shift of Raman Peak from Coated TiO_2 Nanoparticles. *J. Raman Spectrosc.* **2001**, *32*, 862–865. [CrossRef]
27. Parker, J.; Siegel, R. Calibration of the Raman Spectrum to the Oxygen Stoichiometry of Nanophase TiO_2. *Appl. Phys. Lett.* **1990**, *57*, 943–945. [CrossRef]
28. Cheng, X.Q.; Ma, C.Y.; Yi, X.Y.; Yuan, F.; Xie, Y.; Hu, J.M.; Hu, B.C.; Zhang, Q.Y. Structural, Morphological, Optical and Photocatalytic Properties of Gd-Doped TiO_2 Films. *Thin Solid Film.* **2016**, *615*, 13–18. [CrossRef]
29. Ali, T.; Ahmed, A.; Alam, U.; Uddin, I.; Tripathi, P.; Muneer, M. Enhanced Photocatalytic and Antibacterial Activities of Ag-Doped TiO_2 Nanoparticles under Visible Light. *Mater. Chem. Phys.* **2018**, *212*, 325–335. [CrossRef]

30. Zhao, G.; Stevens, S.E. Multiple Parameters for the Comprehensive Evaluation of the Susceptibility of Escherichia Coli to the Silver Ion. *Biometals* **1998**, *11*, 27–32. [CrossRef] [PubMed]
31. Pedahzur, R.; Shuval, H.I.; Ulitzur, S. Silver and Hydrogen Peroxide as Potential Drinking Water Disinfectants: Their Bactericidal Effects and Possible Modes of Action. *Water Sci. Technol.* **1997**, *35*, 87–93. [CrossRef]
32. Spadaro, J.A.; Berger, T.J.; Barranco, S.D.; Chapin, S.E.; Becker, R.O. Antibacterial Effects of Silver Electrodes with Weak Direct Current. *Antimicrob. Agents Chemother.* **1974**, *6*, 637–642. [CrossRef]
33. Campbell, P.N. Principles of Biochemistry Second Edition. *Biochem. Educ.* **1993**, *21*, 114. [CrossRef]
34. Russell, A.D.; Hugo, W.B. 7 Antimicrobial Activity and Action of Silver. In *Progress in Medicinal Chemistry*; Ellis, G.P., Luscombe, D.K., Eds.; Elsevier: Amsterdam, The Netherlands, 1994; Volume 31, pp. 351–370.
35. Liau, S.Y.; Read, D.C.; Pugh, W.J.; Furr, J.R.; Russell, A.D. Interaction of Silver Nitrate with Readily Identifiable Groups: Relationship to the Antibacterialaction of Silver Ions. *Lett. Appl. Microbiol.* **1997**, *25*, 279–283. [CrossRef]
36. Kim, J.S.; Kuk, E.; Yu, K.N.; Kim, J.-H.; Park, S.J.; Lee, H.J.; Kim, S.H.; Park, Y.K.; Park, Y.H.; Hwang, C.-Y.; et al. Antimicrobial Effects of Silver Nanoparticles. *Nanomed. Nanotechnol. Biol. Med.* **2007**, *3*, 95–101. [CrossRef]
37. Feng, Q.; Wu, J.; Chen, G.-Q.; Cui, F.-Z.; Kim, T.; Kim, J. A Mechanistic Study of the Antibacterial Effect of Silver Ions OnEscherichia Coli AndStaphylococcus Aureus. *J. Biomed. Mater. Res.-J. Biomed. Mater. Res.* **2000**, *52*, 662–668. [CrossRef]
38. Matsumura, Y.; Yoshikata, K.; Kunisaki, S.; Tsuchido, T. Mode of Bactericidal Action of Silver Zeolite and Its Comparison with That of Silver Nitrate. *Appl. Environ. Microbiol.* **2003**, *69*, 4278–4281. [CrossRef]